Int. J. Solids Structures Vol. 16, pp. 483–494
Pergamon Press Ltd., 1980. Printed in Great Britain

NUMERICAL STUDIES OF VOID GROWTH IN A NECKED BAR

S. NEMAT-NASSER

Departments of Civil Engineering and Applied Mathematics, Northwestern University, Evanston, IL 60201, U.S.A.

and

M. TAYA

Department of Mechanical and Aerospace Engineering, University of Delaware, Newark, DE 19711, U.S.A.

(*Received* 5 *March* 1979; *in revised form* 6 *August* 1979)

Abstract—For plane strain finite deformation plasticity, several finite-element methods are examined and their corresponding computational efficiency and accuracy are compared by means of an example of pure bending. Then, employing one of the more efficient methods, the state of stress and deformation at the center of a rectangular bar, deformed in uniaxial extension, is studied. On the basis of this information, then the growth process of a (micro) void in a unit cell located at the center of the necked bar, is examined, revealing that the internal fracture at microscopic scales, seems to occur by the formation of shear bands inclined at about 45° with the axis of (macroscopic) extension, a fact which has been observed in ductile fracture of two-phase alloys. Finally, void growth parameters (i.e. those which characterize the geometry of the void) are computed and the results are compared with those obtained from a solution given by McClintock, arriving at a reasonably good agreement.

1. INTRODUCTION

It is commonly accepted that void growth at nonmetallic inclusions in two-phase alloys plays a significant role in the process of ductile fracture, see [1] for a discussion and references. The corresponding plastic flow in the vicinity of the voids involves very large strains of, and exceeding 100%. Deformations of this kind are essentially incompressible, and therefore, numerical methods needed for the analysis must account for this incompressibility [2–5].

In this paper we first present and compare several finite-element methods which have been developed for the analysis of finite plastic deformations in plane strain. By means of an example of pure bending we then estimate the corresponding computational efficiency and accuracy of these methods. Then, employing one of the more efficient methods, we examine the state of stress and deformation at the center of a rectangular bar (plane strain) deformed in uniaxial extension. On the basis of this information, we then study the growth process of a void in a unit cell, revealing that the internal fracture seems to occur by the formation of shear bands inclined at about 45° with the axis of extension, between two adjacent voids, a fact which has been observed experimentally in many situations, see, e.g. [6]. Finally, we compute the void growth parameters (parameters which characterize the geometry of the void) and compare our results with estimates which we obtain from a solution given by McClintock [7]. The present paper, therefore, is complementary to our previous works reported in Ref. [5, 8].

2. FORMULATION OF NUMERICAL METHODS

The considered methods are based on two variational principles which have been presented in [5, 8], and which are summarized below.

2.1 *Variational principles*

Consider the functional J_1 given by

$$J_1(v) = \int_v \left[\frac{1}{2}\frac{\rho}{\rho_0} C_{abce} D_{ab} D_{ce} - T_{ab} D_{ac} D_{cb} + \frac{1}{2} T_{ab} v_{c,a} v_{c,b} - \rho \dot{f}_a v_a\right] \mathrm{d}v$$

$$- \int_s \dot{T}_a v_a \, \mathrm{d}s, \tag{2.1}$$

where repeated indices are summed, and where

$$C_{abce} = \frac{E}{1+\nu}\left\{\delta_{ac}\delta_{be} + \frac{\nu}{1-2\nu}\delta_{ab}\delta_{ce} - \alpha\frac{3}{2}\left(\frac{E}{1+\nu}\right)\frac{T'_{ab}T'_{ce}}{\sigma^2\left(\frac{2}{3}h + \frac{E}{1+\nu}\right)}\right\},$$

$$\frac{\mathcal{D}\tau_{ab}}{\mathcal{D}t} = C_{abce}D_{ce},\ \sigma^2 = \frac{3}{2}T'_{ab}T'_{ab}, \tag{2.2}$$

$$D_{ab} = \frac{1}{2}(v_{a,b} + v_{b,a}).$$

Here dv and ds are volume and surface elements in the current configuration, $\dot{f}_a$ and $\dot{T}_a$ are the prescribed rates of body force (per unit mass) and surface traction (per unit current area), ρ_0 and ρ are mass densities in the initial and current configurations, respectively, T_{ab} are the components of Cauchy's stress, and T'_{ab} is the corresponding deviator. In (2.2), E, ν, and h are, respectively, Young's Modulus, Poisson's ratio, and the work-hardening parameter; $\alpha = 1$ for plastic loading and $\alpha = 0$ for elastic loading or unloading. The quantity $\mathcal{D}\tau_{ab}/\mathcal{D}t$ is the Jaumann rate of the Kirchhoff stress, see Hill[9], Prager[10] and Nemat-Nasser[11].

It is easy to show that the vanishing of the variation of J_1, for arbitrary but kinematically admissible variation in the velocity field, results in the equilibrium equations and traction boundary conditions for the rate problem, see [8].

Next we consider the following functional, J_2, in which independent fields subject to variations are v_a and $\dot{q} = \dot{p}/E$, where $\dot{p}$ is the pressure-rate:

$$J_2 = \int_v \left[\frac{\rho}{\rho_0}\left\{\frac{1}{2}C'_{abce}D_{ab}D_{ce} + \frac{3\nu}{1+\nu}E\dot{q}D_{cc} - \frac{9E\nu(1-2\nu)}{2(1+\nu)}\dot{q}^2\right\}\right.$$
$$\left. - T_{ab}D_{ca}D_{cb} + \frac{1}{2}T_{ab}v_{c,a}v_{c,b} - \rho\dot{f}_a v_a\right] dv - \int_s \dot{T}_a v_a\, ds \tag{2.3}$$

the corresponding constitutive relations are now written as

$$\frac{\mathcal{D}\tau_{ab}}{\mathcal{D}t} = C'_{abce}D_{ce} + \frac{3\nu}{1+\nu}E\dot{q}\,\delta_{ab},$$

$$C'_{abce} = \frac{E}{1+\nu}\left[\delta_{ac}\delta_{be} - \alpha\frac{3}{2}\left(\frac{E}{1+\nu}\right)\frac{T'_{ab}T_{ce}}{\sigma^2\left(\frac{2}{3}h + \frac{E}{1+\nu}\right)}\right] \tag{2.4}$$

$$\dot{q} = \frac{1}{3E}\frac{\mathcal{D}\tau_{cc}}{\mathcal{D}t}.$$

We take the first variation of J_2 with v_a and $\dot{q}$ as independent fields, and use (2.4) to obtain

$$J_2 = \int_v \left[\frac{\rho}{\rho_0}\frac{\mathcal{D}\tau_{ab}}{\mathcal{D}t}\delta D_{ab} - T_{ab}\delta(D_{ca}D_{cb}) + \frac{1}{2}T_{ab}\delta(v_{c,a}v_{c,b}) - \dot{f}_a\delta v_a\right] dv$$
$$- \int_s \dot{T}_a\delta v_a\, ds + \int_v \frac{\rho}{\rho_0}\frac{3\nu E}{(1+\nu)}\{D_{cc} - 3(1-2\nu)\dot{q}\}\delta\dot{q}\, dv. \tag{2.5}$$

The first two integrals on the right-hand side of (2.5) are identical to δJ_1, and the last integral gives the following dilatational constitutive relation:

$$D_{cc} = 3(1-2\nu)\dot{q} \text{ in } v. \tag{2.6}$$

For a strictly incompressibile case ($\nu = 0.5$), functional J_2 can still be used: we set $\nu = 0.5$ in (2.6) and arrive at

$$D_{cc} = 0. \tag{2.7}$$

Functional J_2 represents the rate-form, nonlinear version for elasto-plastic materials of a functional proposed by Herrmann[12] for linear elasticity. Nagtegaal *et al.*[4] derived a somewhat similar functional. The authors in [4] assumed a piecewise constant pressure-rate field, and then eliminated the pressure-rate in order to arrive at a modified strain-displacement relation. Their procedure requires that the material be compressible. Moreover, their method becomes identical with the usual displacement method if a piecewise linear displacement field is used. The numerical formulations based on the J_2 variational principle, on the other hand, remain valid for strictly incompressible materials.

2.2 *Finite-element formulations*

We shall use piecewise linear fields within each element. In our previous report[8], four different methods have been presented and the corresponding results compared. In the present work we shall give two additional methods which have certain advantages over the previous methods. These methods are denoted by A and B. We also consider a modified version of the method 4 given in [8], and denote it by method 4'. For the sake of completeness we shall first list below the methods discussed in [8].

Method 1. This is based on the J_1 functional and triangular elements, and is the same as the usual displacement method. It is effective for compressible materials.

Method 2. This is based on the J_2 functional and uses a linear velocity field and a constant pressure-rate field in each triangle. The final stiffness matrix obtained by this method is not positive definite, so that the usual solution procedure (e.g. Cholesky decomposition) cannot be applied. For compressible materials, Method 2 reduces to Method 1, except it is relatively inefficient and inaccurate.

Method 3. In this method the velocity field as well as the pressure-rate field are taken to be linear over each triangular element. This results in a banded matrix formulation which is appealing, but the additional degrees of freedom renders the computational procedure more expensive.

Method 4. In this method a quadrilateral element with crossed diagonals is used, see Fig. 1. A linear velocity field is considered in each triangle, but *a common constant pressure-rate field is employed for all four triangles* which constitute a given quadrilateral element. The method applies to both compressible and strictly incompressible materials. It appears to be more effective than the other three methods. It is convenient to use different solution schemes for the compressible case and for the strictly incompressible case. The detailed procedure is presented in [8]. We shall denote the procedure for the strictly incompressible case by Method 4'. In both Methods 4 and 4', static condensation is used to eliminate the pressure-rate field in each quadrilateral element.

We shall now consider two additional methods, designated by A and B, which are more effective than those stated above.

Method A. This is based on the J_1 functional, and the quadrilateral element shown in Fig. 1. From $\delta J_1 = 0$ we obtain, for a typical quadrilateral element,

$$\begin{bmatrix} K_{11} & K_{12} \\ K_{12}^T & K_{22} \end{bmatrix} \begin{Bmatrix} v_1 \\ v_2 \end{Bmatrix} = \begin{Bmatrix} \dot{R}_1 \\ \dot{R}_2 \end{Bmatrix}, \tag{2.8}$$

where the subscript 1 refers to the outer vertices, and the subscript 2 to the inner vertex of the

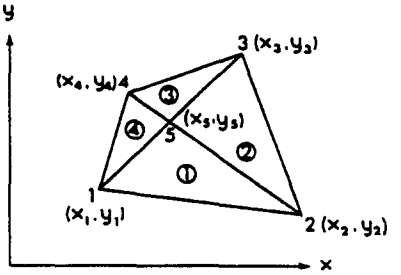

Fig. 1. A special quadrilateral element.

typical element shown in Fig. 1. We now perform a static condensation on (2.8), to obtain

$$Kv_1 = \dot{R}, \tag{2.9}$$

where matrix K and vector $\dot{R}$ are given by

$$K = K_{11} - K_{12}K_{22}^{-1}K_{12}^T,$$
$$\dot{R} = \dot{R}_1 - K_{12}K_{22}^{-1}\dot{R}_2. \tag{2.10}$$

After (2.9) is assembled into a global matrix, we solve for v_1 corresponding to vertices of all the quadrilateral elements. In order to compute the average strain-rate, $\bar{D}_{ab}$, over the four triangles which form a typical quadrilateral element, we use the following relation:

$$\bar{D} = \bar{B}\begin{Bmatrix} v_1 \\ v_2 \end{Bmatrix}, \quad \bar{B} = \frac{1}{4}\sum_{i=1}^{4} B^i, \tag{2.11}$$

where B^i, $i = 1,2,3,4$, are the matrix coefficients for the corresponding strain-rate, velocity-relations, pertaining to the constituent triangles. The average stress-rate, $\mathring{\mathcal{D}}\bar{\tau}_{ab}/\mathcal{D}t$, is computed with the aid of $(2.2)_2$, and the nodal forces are obtained from

$$\dot{R} = \hat{B}T, \quad \hat{B} = \sum_{i=1}^{4}\int_{A^i} B^{iT}\,\mathrm{d}A^i, \tag{2.12}$$

where T is the Cauchy stress, and A^i denotes the area of the ith triangle in a typical quadrilateral element. For the purpose of iteration, the nodal forces corresponding to the inner point of a quadrilateral element, are condensed with the aid of $(2.10)_2$.

Method B. We apply the functional J_2 to a typical quadrilateral element, denoted by β, assuming that the pressure-rate, $\dot{q}_\beta$, is constant, and that the velocity field, v, is linear in each triangle. With the aid of (2.5) and noting that $\delta\dot{q}_\beta$ is arbitrary, we obtain

$$\dot{q}_\beta = \sum_{i=1}^{4} D_{cc}^i A_\beta^i/\{3(1-2\nu)A_\beta\} \quad (\beta \text{ not summed}), \tag{2.13}$$

where the superscript i refers to the ith triangle in the βth element, A_β^i is the initial area of this triangle, and A_β is the initial area of the βth element.

We now apply J_2 to the entire body, enter the value of the pressure-rate for each element from (2.13), and from $\delta J_2 = 0$ obtain

$$Kv_\beta = \dot{R} \tag{2.14}$$

for the βth element; here the five dimensional vector v_β denotes collectively the nodal velocities of the βth element, and K and $\dot{R}$ are given by

$$K = \sum_{i=1}^{4}\left\{\int_{A^i}\left[\frac{\rho^i}{\rho_0}B^{iT}C^{ri}B^i + M^{iT}\sigma^i M^i - 2\mathring{M}^{iT}\sigma^i\mathring{M}^i\right]\mathrm{d}A_\beta^i + \sum_{i=1}^{4} E\nu(NN^iA_\beta^i)^2/\{(1+\nu)(1-2\nu)A_\beta\}, \tag{2.15}$$

$$\dot{R} = \sum_{i=1}^{4}\left\{\int_{A_\beta^i}\rho^i N^{iT}\dot{f}^i\,\mathrm{d}A_\beta^i + \int_{L_\beta^i} N^{iT}\dot{T}^i\,\mathrm{d}L_\beta^i\right\}; \tag{2.16}$$

in these expressions the matrices NN^i and N^i are such that

$$D_{cc} = NN^i v_\beta, \quad v^i = N^i v_\beta, \tag{2.17}$$

M^i and $\mathring{M}^i$ are functions of the coordinates of the nodal points in the current configuration for

the ith triangle in the βth element, and

$$\sigma^i = \begin{bmatrix} T^i & 0 \\ 0 & T^i \end{bmatrix}, \quad T^i = \begin{bmatrix} T^i_{11} & T^i_{12} \\ T^i_{12} & T^i_{22} \end{bmatrix}. \tag{2.18}$$

On the other hand, if we do not eliminate the pressure-rate, $\dot{q}_\beta$, we obtain, for the βth element,

$$\begin{bmatrix} K_{vv} & K_{vq} \\ K^T_{vq} & K_{qq} \end{bmatrix} \begin{Bmatrix} v_\beta \\ \dot{q}_\beta \end{Bmatrix} = \begin{Bmatrix} \dot{R} \\ 0 \end{Bmatrix}, \tag{2.19}$$

where

$$K_{vv} = \sum_{i=1}^{4} \int_{A_\beta{}^i} \left[\frac{\rho^i}{\rho_0{}^i} B^{iT} C'^i B^i + M^{iT} \sigma^i M^i - 2\mathring{M}^{iT} \sigma^i \mathring{M}^i \right] \mathrm{d}A_\beta{}^i, \tag{2.20}$$

$$K_{vq} = \frac{3\nu E}{1+\nu} N \sum_{i=1}^{4} N^i A_\beta{}^i, \quad K_{qq} = \frac{9\nu E(1-2\nu)}{(1+\nu)} A_\beta, \tag{2.21}$$

with $\dot{R}$ defined by (2.16). If the material is not strictly incompressible, we can eliminate $\dot{q}_\beta$ in (2.19) to obtain

$$[K_{vv} + K_{vq} K^{-1}_{qq} K^T_{vq}] v_\beta = \dot{R}. \tag{2.22}$$

It can easily be verified that

$$K = K_{vv} + K_{vq} K^{-1}_{qq} K^T_{vq}, \tag{2.23}$$

and, therefore, we arrive at (2.14) which involves fewer degrees of freedom than included in (2.19), the total number of the degrees of freedom being equal to those in the corresponding displacement-based finite-element Method A.

We now examine when (2.14) would indeed be identical with the corresponding system of equations obtained from the displacement-based variational principle. To this end, we replace C'_{abce} in J_2 by $C_{abce} - E\nu\delta_{ab}\delta_{ce}/\{(1+\nu)(1-2\nu)\}$ and obtain

$$J_2 = J_1 + \sum_\beta \sum_{i=1}^{4} \frac{1}{2} \frac{\rho}{\rho_0} \frac{E\nu}{(1+\nu)(1-2\nu)} \left[\frac{(D^i_{cc} A_\beta{}^i)^2}{A_\beta} - (D^i_{cc})^2 A_\beta{}^i \right]. \tag{2.24}$$

Thus J_2 would be identical with J_1 if $D^1_{cc} = D^2_{cc} = D^3_{cc} = D^4_{cc}$, i.e. when the dilatational strain-rate is uniform over all four triangles which form the βth element. However, since the velocity field is linear over each triangle, the corresponding strain-rate is constant, in general having a *different value* in each triangle.

All the foregoing methods are implemented incrementally using the Newton–Raphson iteration method; the Newton–Raphson iteration is performed during each increment until convergence is obtained, and for the first two iterations the stiffness matrix is updated in order to take into account the rapid change in the slope of the load-deflection curve. This rapid change occurs when an element experiences elasto-plastic transition. On the other hand, when the load-deflection curve becomes "flat" in almost every element, the appropriate acceleration scheme is used to speed up the convergence.

3. NUMERICAL RESULTS

Before presenting numerical results for the problem of the void growth at the center of a necked bar, we consider the simple example of pure bending of a beam, in order to compare the accuracy and the corresponding computational efficiency of the various considered methods.

3.1 *Pure bending of an elastic–plastic beam*

We assume that plane sections perpendicular to the beam's axis remain plane during the deformation, and consider a slice of unit thickness subjected to the prescribed displacement,

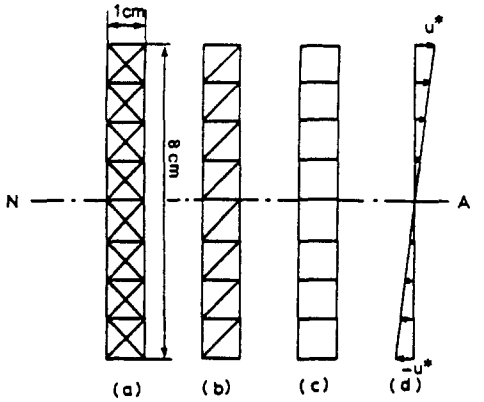

Fig. 2. Finite-element systems for pure bending.

u^*, as shown in Fig. 2. For Methods 4 and 4′ we have used the finite-element mesh shown in Fig. 2(a), for Method 1, the finite-element 2b, and for Methods A and B, the finite-element 2c are, respectively, used, where in 2c, the central node is condensed. We increased the curvature incrementally, using equal increments of 10^{-5}, until the moment-curvature curve attains a constant slope. The material properties of the beam are, $E = 3 \times 10^7$ Kg/cm, $\sigma_y = 3.5 \times 10^4$ Kg/cm^2, h (work hardening parameter) $= 5.0 \times 10^4$ Kg/cm^2, and $\nu = 0.3$. For this choice of the material properties the pseudo-analytical solution for the constant slope is given by

$$\frac{M}{\sigma_y H^2}/\frac{K}{K_e} = 0.0003741, \tag{3.1}$$

where M is the bending moment, H is the thickness of the beam, K is the curvature corresponding to M, and K_e is the curvature for which the outer fiber of the beam becomes plastic for the first time. The numerical solutions for the constant slope, normalized by the corresponding pseudo-analytical solution, are given in Table 1, together with the computational time normalized with respect to the time required to implement Method A. This table also shows the type of finite-element used. The dashed line for the type of elements used for Methods A and B indicates that the central node has been condensed. It is seen that Methods 4 and 4′ give the vest accuracy for both compressible and incompressible materials, for Methods A, B, 1 and 4, $\nu = 0.49$ is used to simulate the incompressible case (it is therefore "almost" incompressible). On the other hand, Methods A and B yield fairly accurate results with least computational time.

Table 1. Numerical results for the limit slope in pure bending normalized by the analytical solution ($\nu = 0.3$ and $\nu = 0.5$); together with the corresponding computational time for various methods normalized by Method A

		The present methods		The previous methods		
		Method A	Method B	Method 1	Method 4	Method 4′
		displacement (condensed)	Mixed $\dot{q}$ = const. $\dot{q}$ and displ. condensed	displacement	Mixed $\dot{q}$ = const. ($\dot{q}$ condensed)	Mixed $\dot{q}$ = const. (strictly incompressible)
Poisson's ratio ν	types of element	⊠ △	⊠ △	△	⊠	⊠
0.3	limiting slope in pure bending	1.012	1.010	1.035	0.999	
0.5 (0.49 for Methods A, B, 1 and 4)		1.014	1.013		0.999	0.998
0.3	computation time normalized by Method A	1.0	1.063	0.997	1.260	
0.5 (0.49 for Methods A, B, 1 and 4)		1.0	1.063		1.262	1.437

In the sequel we shall consider first, the necking of a smooth bar in extension and calculate the corresponding field quantities by means of Method 1. We then use these results to study the process of void growth at the center of such a bar, using Method A.

3.2 *Necking of an elasto-plastic bar in plane strain*

The necking of a rectangular bar with an initial imperfection at its central portion, is analyzed numerically by Method 1. The bar consists of an elasto-plastic work-hardening material, obeying a power-hardening law given by

$$\epsilon = \begin{cases} \dfrac{\sigma}{E} & \text{if} \quad \sigma \leqslant \sigma_y \\ \dfrac{\sigma^n}{E\sigma_y^{n-1}} & \text{if} \quad \sigma \geqslant \sigma_y, \end{cases} \tag{3.2}$$

where σ and ϵ are the effective true stress and strain, respectively, and σ_y is the yield stress. The material properties of the bar are the same as those used in Subsection 3.1 except for the work-hardening parameter h which is not constant here, but depends on σ and n ($=8$). The finite-element mesh and the geometry of the bar are shown in Fig. 3. The problem of necking in a bar, using finer mesh systems and for a bilinear elasto-plastic material, has been solved numerically by Osias[13] and McMeeking and Rice[14]. Here we compute the distribution of stresses, strains, and a triaxiality parameter along the center line (the x_2-axis in Fig. 3), as well as the profile of the necked bar. A total displacement of $u^* = 6$ cm is applied incrementally at one end of a quarter of the tensile specimen. Three stages of the necked profile with the corresponding boundaries between the elastic (unloaded) and plastic regions are shown in Fig. 4, where the dotted line denotes the initial profile of the bar. The Cauchy stress components along the line parallel to the central section (the x_2-axis) at the center of the quadrilateral elements are shown in Fig. 5. Note that, since the average value of stress calculated at the

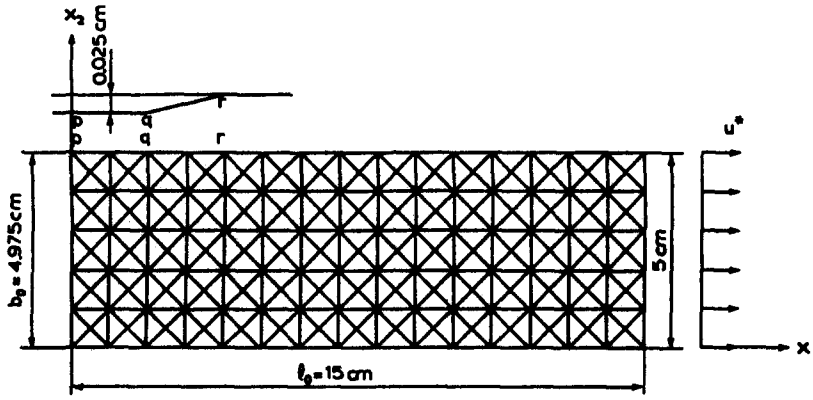

Fig. 3. One quarter of a bar with initial imperfection subjected to prescribed displacement u^*, plane strain.

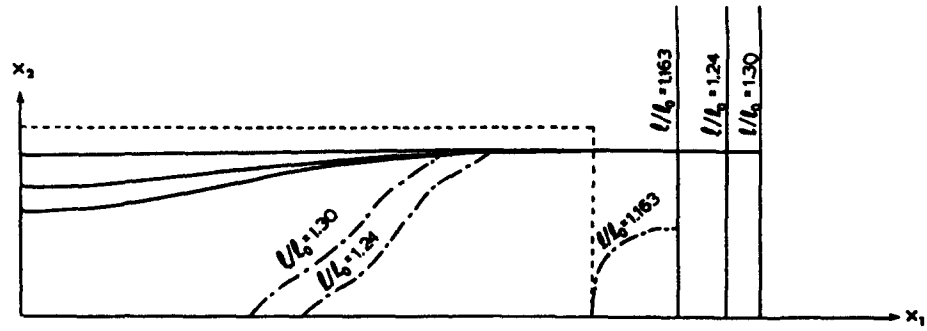

Fig. 4. The necked profile of a bar (solid curves) and propagation of the unloading area (bounded by dash-dot curves).

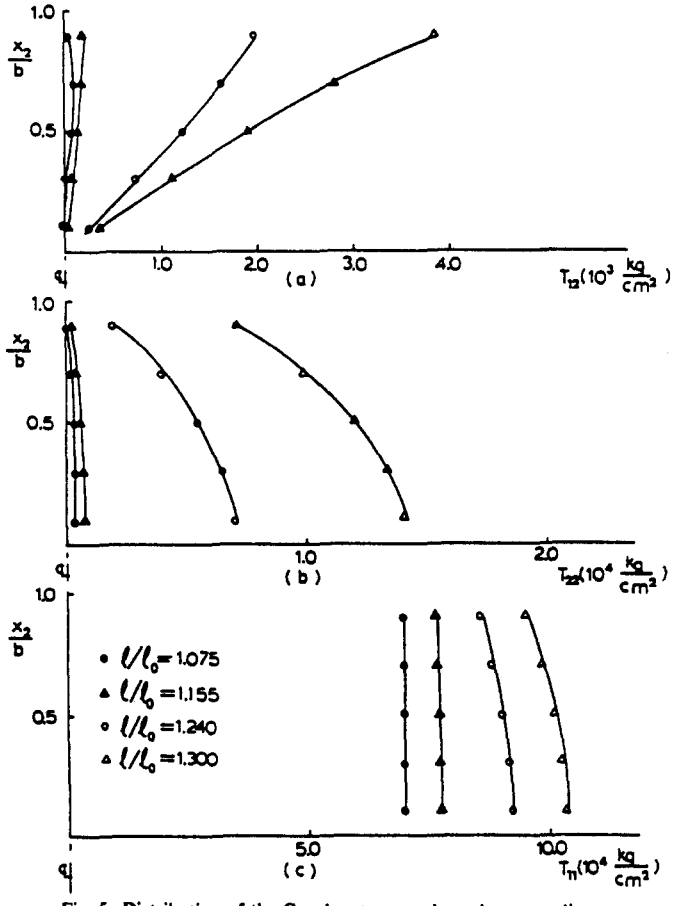

Fig. 5. Distribution of the Cauchy stresses along the center line.

center of each quadrilateral element is assigned to each element, T_{12} has a finite value in the vicinity of $x_2/b = 1$; note, however, that the horizontal scales for the three stress components in Fig. 5 are not the same. The black and open marks in Fig. 5 correspond to the before and after of the onset of unloading, respectively; the same notation is used in Fig. 6. The distribution of the nominal strains, ϵ_{11} and ϵ_{22}, and the equivalent plastic strain ϵ_p along the center line is shown in Figs. 6(a)–(c), from which a rather flat gradient for the strains is observed. Bridgman's[15] assumption of a constant ϵ_p along the center line is approximately verified for small values of the elongation, l/l_0, as is seen in Fig. 6(a). Recent studies, e.g.† [6 and 7], have shown that the traxiality parameter β, i.e. the ratio of the mean stress to the flow stress, plays an important role in the mechanism of void growth in ductile fracture. Therefore we have plotted β and $|\epsilon_{22}|/\epsilon_{11}$ at the center of the bar as functions of l/l_0 in Fig. 7. It is observed that the triaxiality parameter β is constant before the onset of unloading (indicated by a vertical line U in Fig. 7), and increases at a constant rate after unloading sets in. On other hand the quantity $|\epsilon_{22}|/\epsilon_{11}$, decreases continuously as l/l_0 increases. In the sequel we shall use these results in order to investigate the mechanism of microscopic void growth at the center of a tensile specimen.

3.3 *Void growth at the center of a necked bar*

We shall now study the process of the growth of a void at the center of the necked bar (plane strain). For the calculation we use Method A, and subject a void (10μ, radius) in a unit cell (100μ) at its boundary to the history of the deformation defined by the values of ϵ_{11} and ϵ_{22} at the center of the tensile bar, given in Fig. 7. One quarter of the unit cell is shown in Fig. 8, together with the corresponding finite-element mesh. The matrix material has the same properties as those of the tensile bar in the preceding section.

†For additional references, see [16].

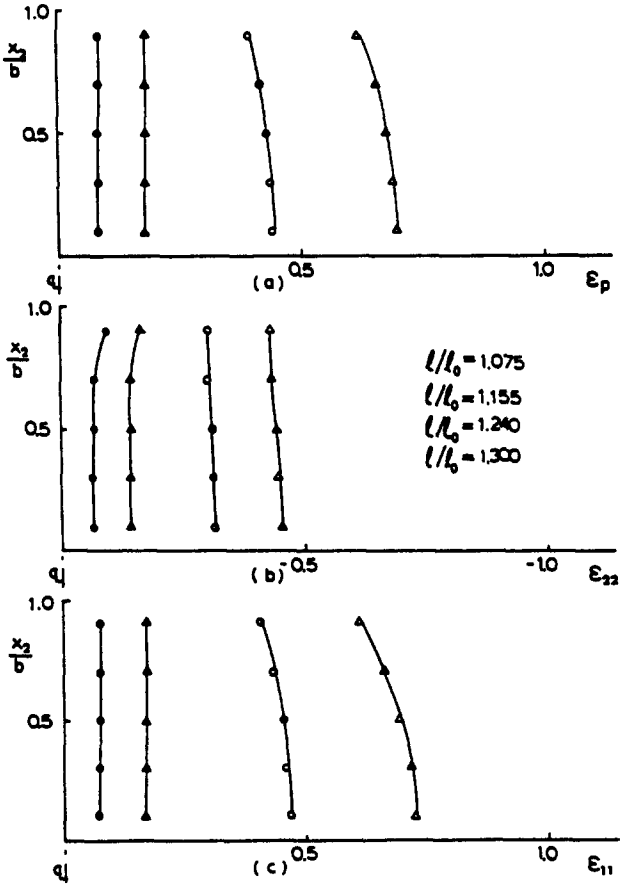

Fig. 6. Distribution of equivalent plastic strain, ϵ_p, and nominal strains, ϵ_{11} and ϵ_{22}, along the center line.

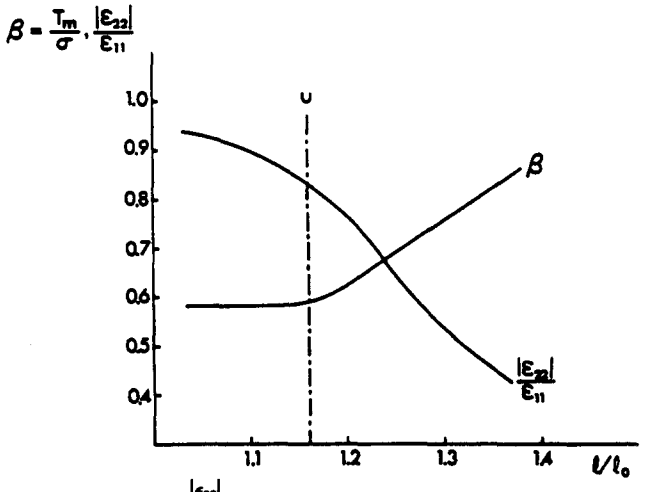

Fig. 7. $\frac{|\epsilon_{22}|}{\epsilon_{11}}$ and triaxiality parameter β vs l/l_0.

The cell is subjected to uniformly distributed prescribed displacements, u^* and v^*, corresponding to the local strains, ϵ_{11} and ϵ_{22}, at the center of the necked bar. In Fig. 9 we have reported the resultant force in the x_1-direction, T_1, acting on the unit cell, and the average mean stress, T_m, on the x_2-boundary, as functions of ϵ_{11}. In Figs. 10 and 11 respectively, we have shown contour lines of constant effective plastic strain, ϵ_p, and maximum shear stress (normalized by dividing by σ_y) at the stage of deformation which corresponds to the macroscopic

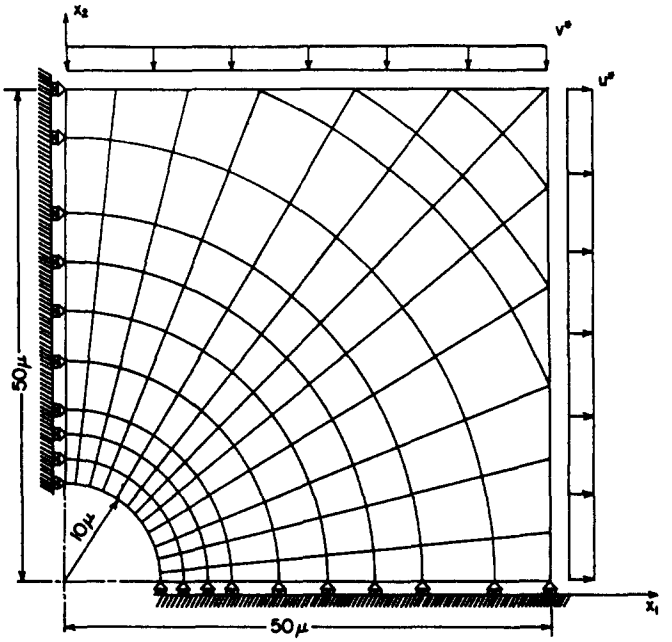

Fig. 8. Finite-element mesh and geometry of a unit cell.

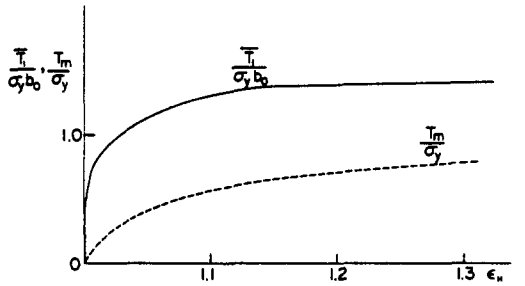

Fig. 9. The resultant force $\bar{T}_1/\sigma_y b_0$, and the average mean stress, T_m/σ_y, as functions of axial nominal strain ϵ_{11}.

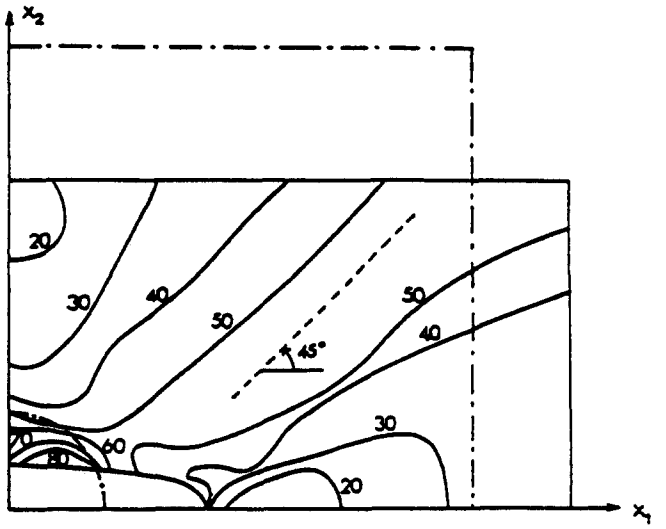

Fig. 10. Contours of constant effective plastic strain, ϵ_p, for macroscopic strain of $\epsilon_{11} = 0.4$.

strain of $\epsilon_{11} = 0.4$. The dash-dot lines in these figures mark the initial geometry of the unit cell. From these figures it is seen that a region of intense plastic flow forms at a 45° angle with the x_1-axis. If the material contains, in addition to large microscopic particles, small precipitates (less than 0.1μ) distributed throughout the matrix, then one would expect that small voids

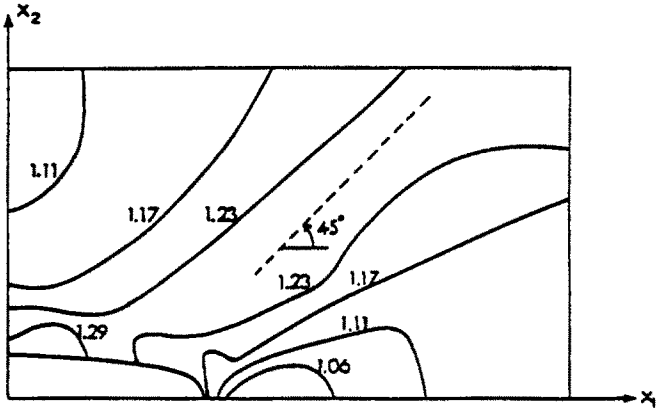

Fig. 11. Contours of maximum shear stress (divided by σ_y) for macroscopic strain of $\epsilon_{11} = 0.4$.

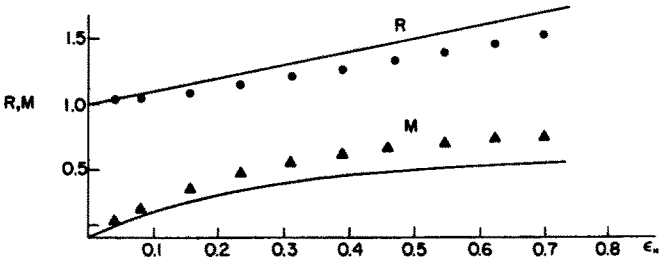

Fig. 12. Void growth parameters R and M vs ϵ_{11}.

would nucleate at these particles in the region between the 50% strain contours shown in Fig. 10. Thus it is reasonable to conclude that adjacent larger microvoids in this case may be connected by "void sheets" at a certain stage of straining, marking the incipience of ductile fracture.

It should be noted, however, that the existence of voids, and the fact that intense shear deformations occur between adjacent voids, render the macroscopic response of the bar *plastically compressible*. Our calculations in Section 3.2 do not include plastic compressibility. A satisfactory constitutive relation for finite plasticity with compressibility and encompassing a nonassociative flow-rule, recently has been developed by Nemat-Nasser and Shokooh[17], but the application of the theory to the problem of the necking of a bar has not yet been made.

Finally, we have reported in Fig. 12 the void growth parameters defined by

$$R = \frac{1}{2}(r_1 + r_2),\ M = (r_1 - r_2)/(r_1 + r_2), \tag{3.3}$$

as functions of ϵ_{11}, where r_1 and r_2 are the radii of the void in the x_1-and x_2-directions, respectively. In this figure the solid curves are obtained from McClintock's[7] analytical solutions (see Appendix A), and the corresponding geometrical marks are our numerical results. It is seen that reasonably good agreement exists between these results. The relevant details for the application of McClintock's solutions (which is based on analytical work of Berg[18]) to our problem, are summarized in Appendix A.

Acknowledgement—This work has been supported by the National Science Foundation under Grant No. ENG-76-03921 to Northwestern University.

REFERENCES

1. G. T. Hahn, M. F. Kanninen and A. R. Rosenfield, Fracture toughness of materials. *Ann. Rev. Mat. Sci.* 2, 381–404 (1972).
2. J. H. Argyris, P. C. Dunne, T. Angelopoulos and B. Bichat, Large natural strains and some special difficulties due to non-linearity and incompressibility in finite elements. *Comp. Meths. Appl. Mech. Engng.* 4, 219–278 (1974).
3. J. H. Argyris, P. C. Dunne, Th.L. Johnsen and M. Müller, Linear systems with a large number of sparse constraints with application to incompressible materials. *Comp. Meths. Appl. Mech. Engng.* 10, 105–132 (1977).

4. J. C. Nagtegaal, D. M. Parks and J. R. Rice, On numerically accurate finite element solutions in the fully plastic range. *Comp. Meths. Appl. Mech. Engng.* 4, 153–177 (1974).
5. S. Nemat-Nasser and M. Taya, Model studies of ductile fracture- I. Formulation. *J. Franklin Institute*, Basis of the Finite Element Method **302**, 463–472 (1976).
6. T. B. Cox and J. R. Low Jr., An investigation of the plastic fracture of AISI 4340 and 18 Nickel-200 grade maraging steels. *Metallurg. Trans.* 5, 1457–1470 (1974).
7. F. A. McClintock, A criterion for ductile fracture by the growth of holes. *J. Appl. Mech.* **35**, 363–371 (1978).
8. S. Nemat-Nasser and M. Taya, model studies of ductile fracture—Part II: Further Numerical Formulations, *Proc. Int. Conf. on Finite Elements in Nonlinear Solid and Structural Mechanics*, (Edited by P. G. Bergan *et al*), Vol. 1 211–239. TAPIR Publishers, Norwegian Institute of Technology, Trondheim, (1978).
9. R. Hill, Eigenmodel deformation in elastic-plastic continua. *J. Mech. Phys. Solids* **15**, 371–386 (1967).
10. W. Prager, Introduction to mechanics of continua, (Ginn, Boston, 1961).
11. S. Nemat-Nasser, Continuum basis for consistent numerical formulations of finite strains in elastic and inelastic structures, *Finite Element Analysis of Transient Nonlinear Structural Behavior*, (Edited by T. Belytschko *et al.*) ASME, AMD-14 PP. 85–98 (1975).
12. L. R. Herrmann, Elasticity equation for incompressible and nearly incompressible materials by a variational theorem. *AIAA J.* 3, 1896–1900 (1965).
13. J. R. Osias, Finite deformation of elastic-plastic solids. *NASA* Cr-2199 (1973).
14. R. M. McMeeking and J. R. Rice, Finite-element formulations for problem of large elastic-plastic deformation, *Int. J. Solids Structures* **11**, 601–616 (1975).
15. P. W. Bridgman, *Studies in Large Plastic Flow and Fracture.* McGraw-Hill, New York (1952).
16. S. Nemat-Nasser, Overview of the basic progress in ductile fracture, *Transactions* 4th *Int. Conf, on Struct. Mech. in Reactor Technology*, San Francisco, Cal., Vol. L (1977) L2/1* 1–11 (Aug. 1977).
17. S. Nemat-Nasser, and A. Shokooh, On finite plastic flows of compressible materials with internal friction. Earthquake Research and Engineering Lab., *Tech. Rep.* No. 79-5-16, Dept. of Civil Engr., Northwestern University, Evanston, IL., May 1979; to appear in *Int. J. Solids Structures.*
18. C. A. Berg, The motion of cracks in plane viscous deformation, *Proc* 4th *U.S. National Congress of Appl. Mech. ASME* 2, 885–892 (1962).

APPENDIX A

Based on Berg's analytical solution[20] for the growth of an elliptical hole in ϵ viscous material, MacClintock[7] obtained for an elasto-plastic material, the following expressions for the void growth parameters (i.e. for the mean radius R and the eccentricity M):

$$\ln\left(\frac{R}{R_0}\right) = \frac{\epsilon\sqrt{3}}{2(1-n)} \sinh\left\{\frac{\sqrt{3}(1-n)}{2}\frac{\sigma_{11}+\sigma_{22}}{\sigma}\right\} + \frac{\epsilon_{11}+\epsilon_{22}}{2}, \tag{A1}$$

$$M = \frac{\sigma_{11}-\sigma_{22}}{\sigma_{11}+\sigma_{22}} + \left(M_0 - \frac{\sigma_{11}-\sigma_{22}}{\sigma_{11}+\sigma_{22}}\right)\exp\left\{-\frac{\sqrt{3}\epsilon}{(1-n)}\sinh\left(\frac{\sqrt{3}(1-n)}{2}\times\frac{\sigma_{11}+\sigma_{22}}{\sigma}\right)\right\}, \tag{A2}$$

where n is the work-hardening parameter in

$$\sigma = \sigma_0\epsilon^{-n}, \tag{A3}$$

R_0 and M_0 are the initial mean radius and eccentricity, and σ_{11} and σ_{22}, and ϵ_{11} and ϵ_{22} are the principal stresses and strains, respectively.

In the case of the necked tension bar the ratio between stresses is a function of ϵ. Therefore we modify (A1) and (A2) into the differential form,

$$\frac{dR}{R} = \frac{\sqrt{3}}{2(1-n)}d\epsilon \sinh\left\{\frac{\sqrt{3}}{2}(1-n)\frac{\sigma_{11}+\sigma_{22}}{\sigma}\right\} \tag{A4}$$

$$dM = -\frac{\sqrt{3}}{(1-n)}\left\{M - \frac{\sigma_{11}-\sigma_{22}}{\sigma_{11}+\sigma_{22}}\right\}\sinh\left\{\frac{\sqrt{3}(1-n)}{2}\frac{\sigma_{11}+\sigma_{22}}{\sigma}\right\}d\epsilon \times \exp\left\{-\frac{\sqrt{3}\epsilon}{(1-n)}\sinh\left(\frac{\sqrt{3}(1-n)}{2}\frac{\sigma_{11}+\sigma_{22}}{\sigma}\right)\right\}. \tag{A5}$$

In deriving (A4) and (A5), we assume that n and the ratio of stresses remain constant. In order to use the differential forms (A4) and (A5), we divide ϵ into 8 increments, and during each increment use the constant stress-ratio and n which are already obtained from the necked tension bar. We follow McClintock in computing a work-hardening parameter n, which is

$$n = \frac{\sigma(\text{at } \epsilon)}{\sigma_{\text{average}}(\text{up to } \epsilon)} - 1. \tag{A6}$$